ADVANCED MATERIALS

Efficient Infrared-Emitting PbS Quantum Dots Grown on DNA and Stable in Aqueous Solution and Blood Plasma**

By *Larissa Levina*, *Vlad Sukhovatkin*, *Sergei Musikhin*, *Sam Cauchi*, *Rozalia Nisman*, *David P. Bazett-Jones*, and *Edward H. Sargent**

Quantum-dot nanocrystals have been used to label single molecules during living-cell assays[1] and provide direct visual guidance and real-time confirmation of complete resection during cancer surgery in an animal model.[2] The use of quantum dots for deep-tissue imaging accompanied by low autofluorescence in vivo requires emission in the second infrared biological window of 1000–1200 nm combined with stability in biological media. Surface chemistry determines the chemical and optical stability of quantum dots. A stabilizing outer shell minimizes diffusion of oxygen to the surface of the core of the nanoparticle, as demonstrated using a high-bandgap semiconductor shell[3] and a dielectric shell.[4] Silanized nanoparticles have been shown to be water soluble and to retain the absorption and emission spectra of the original particles; however, the nanoparticles lost 60–80 % of their original quantum efficiency in this process. Recently, oligomeric phosphines[5] have been employed to form three thin concentric sublayers around quantum dots: an inner phosphine layer for dot-surface passivation, a linking layer for protection, and an outer functionalized layer for miscibility and subsequent chemical modification or conjugation to biomolecules. In the infrared, the application of this multistep synthetic method to type-II core–shell nanoparticles has resulted in quantum dots that show modest degradation in 37 °C plasma over the course of half an hour.[3]

Here we adopt an entirely different strategy: we report the first growth of efficient infrared photoluminescent quantum dots directly on a DNA template. Our infrared-emitting quantum dots grown on the biomolecular template are efficient and stable in water, serum, and blood plasma.

DNA has previously been decorated with metal nanoparticles 5–10 nm in diameter through the use of thiol linkages.[6] DNA has also been used as a long-term stabilizer and template in the growth of CdS nanocrystals, but with no reports of a photoluminescence quantum efficiency.[7–10] Related progress has also been made in synthesizing CdS nanoparticles in which growth was carried out at room temperature followed by annealing at 80 °C to improve photoluminescent properties; quantum efficiencies of 10^{-4} were estimated.[11] The only previous report of DNA-templated growth on PbS has yielded materials with no detectable luminescence in the infrared.[12]

We worked instead at a synthesis temperature at which chemical interaction was possible between the metal cations used in PbS growth and at least two classes of sites on DNA: the phosphate backbone, and also DNA's purine and pyrimidine bases. The bases provide an additional opportunity for control over the growth of nanoparticles and the passivation of their surface states. The synthesis reported herein is simple, reproducible, and yields PbS nanoparticles with exceptional stability and photoluminescence quantum efficiency. Energy-filtered transmission electron microscopy (EFTEM) reveals cubic-latticed PbS quantum dots 4 nm in diameter on a network of DNA. We obtain photoluminescence quantum efficiencies of up to 11.5 %. Aged in standard plasma at 37 °C, the DNA-grown PbS nanocrystals exhibit a quantum-efficiency half-life of one week. We fabricate thin solid films with high optical quality and better than 4 nm surface roughness, and we find that, in contrast to organometallic-route nanocrystals, solution-synthesized DNA-grown PbS nanocrystals retain their high quantum efficiency when fabricated into solid-state films.

The synthesis (see Experimental for details) began with heating the DNA solution for 20 min under nitrogen at temperatures ranging in our experiments from 20 to 100 °C. The DNA solution was maintained at temperature, and lead nitrate was added to it dropwise over 20 min to avoid DNA coagulation. Sodium sulfide was added by single injection, producing a dark red solution.

Dark-field transmission electron microscopy (TEM) was carried out on a sample synthesized with highly polymerized, calf-thymus DNA and subsequently dried onto a carbon grid (Fig. 1a). The average nanoparticle diameter was estimated to be 3.9 nm based on analysis of several images. We observed a cubic diffraction pattern in the bright field, as shown in Figure 1b, where the magnified nanocrystalline region dominates the field of view. X-ray absorption spectroscopy confirmed the presence of Pb and S.

We employed EFTEM, also referred to as electron spectroscopic imaging (ESI), to determine the elemental composition.[13] We identified DNA strands in the field of view and confirmed the presence of nanocrystals on individual DNA strands. By acquiring images at energies corresponding to the post-ionization edge of phosphorus, a phosphorus-enhanced map was created (Fig. 2a). DNA is seen to form a network of elongated filaments. Due to the proximity of the sulfur ionization edge to that of phosphorus, the nanocrystals appear as bright dots within the phosphorus-enhanced image. Some of the quantum dots are far apart along a DNA strand (arrow), whereas others are in close proximity (arrowhead). This is

[*] Prof. E. H. Sargent, L. Levina, V. Sukhovatkin, Dr. S. Musikhin, S. Cauchi
Department of Electrical and Computer Engineering
University of Toronto, 10 King's College Road
Toronto, ON M5S 3G4 (Canada)
E-mail: ted.sargent@utoronto.ca
Dr. R. Nisman, Prof. D. P. Bazett-Jones
Programme in Cell Biology, The Hospital for Sick Children
555 University Avenue, Toronto, ON M5G 1X8 (Canada)

[**] The authors thank Sean Hinds for his assistance in acquiring the dark-field TEM image shown in Figure 1a.

  DOI: 10.1002/adma.200401197

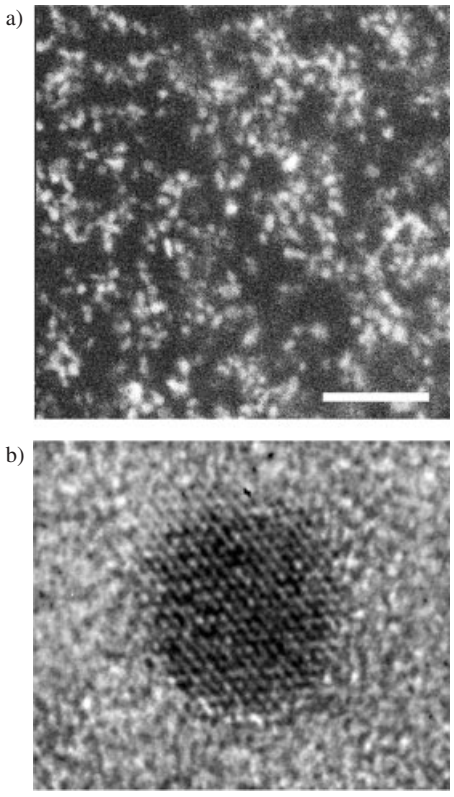

Figure 1. Transmission electron micrographs of DNA-grown PbS nanocrystals. a) Dark-field TEM acquired at 200 kV. Scale bar is 40 nm. Average nanoparticle size is approximately 4 nm. b) Higher-magnification TEM image of a single nanocrystal showing its lattice structure.

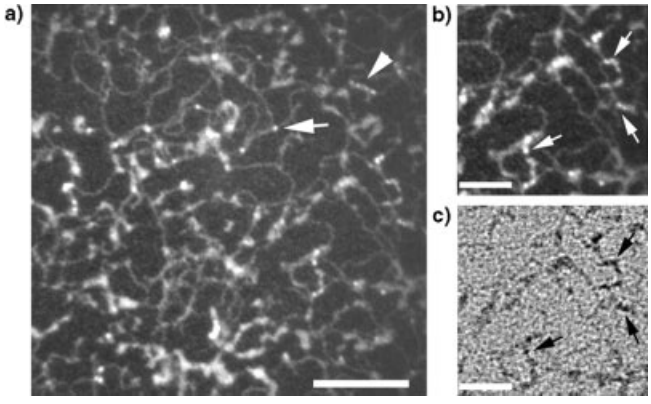

Figure 2. Energy-filtered TEM of DNA-grown PbS nanocrystals. a) Phosphorus-enhanced micrograph illustrates the network of elongated DNA strands. Arrow: nanocrystals associated with DNA appear as bright spots. Arrowhead: a strand with high loading of nanocrystals. Scale bar is 100 nm. b) Enlarged view of a region from (a), and c) its corresponding bright-field image, demonstrating that the electron-dense objects in bright field correspond to bright spots in the phosphorus-enhanced image. Arrows point to regions that have high quantum dot nanocrystal populations within strands of DNA. Scale bars are 50 nm.

readily apparent in the enlarged view (Fig. 2b). The dark spots highlighted with arrows in the corresponding bright-field TEM image (Fig. 2c) correlate to the bright spots apparent in the phosphorus-enhanced map. This confirms that these are electron-dense structures, consistent with nanocrystals. As no contrast agents are employed, the DNA gives negligible contrast in the bright-field image yet shows up clearly as elongated strands in the energy-loss micrograph.

Fluorophores for biological applications must exhibit large absolute photoluminescence quantum efficiencies, and this must be stable over time in relevant biological solutions. We used the spectrally resolved integrating-sphere method (see Experimental) to quantify photoluminescence quantum efficiencies. As shown in Figure 3a, excitonic features are absent from absorption spectra. Similar observations have previously

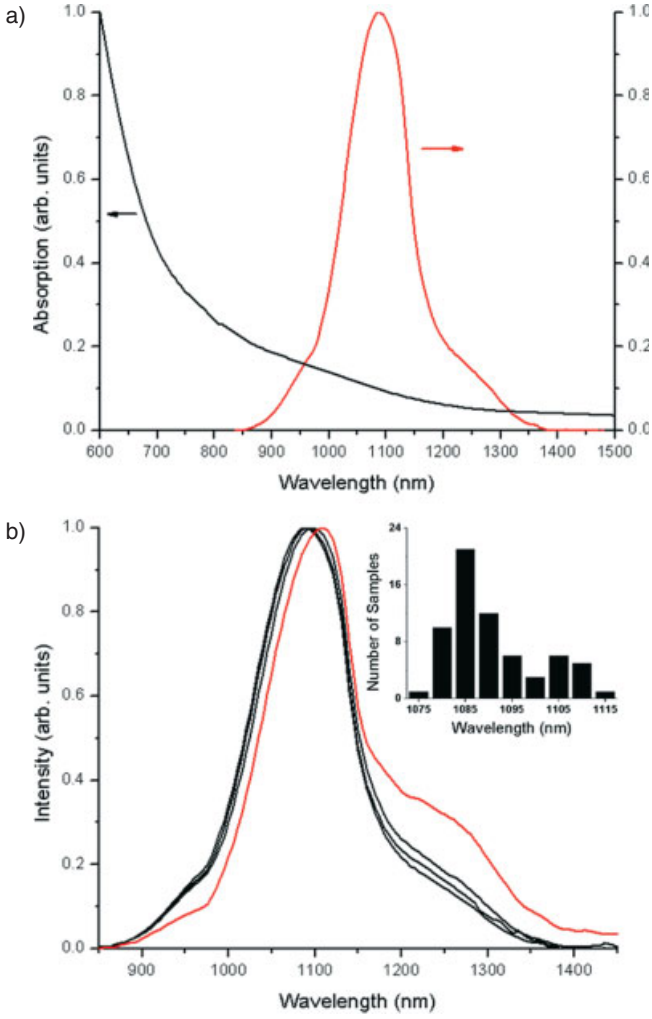

Figure 3. Optical properties of DNA-grown PbS nanocrystals. a) Photoluminescence spectrum of a typical DNA–PbS solution (red) under 830 nm excitation, along with the absorption spectrum (black) of a film created from the same solution. The absorption spectrum was taken in the solid state to avoid water absorption. The solution was synthesized at 93 °C. b) Photoluminescence spectra of aqueous solution samples synthesized at room temperature (red, 7 h incubation period) or between 70 and 95 °C (black, 20 min incubation period). Inset: Histogram created using the photoluminescence spectra of 65 solution samples. This illustrates the reproducibility of the photoluminescence peak position. See text for details.

ADVANCED MATERIALS

been made in other aqueous-synthesized PbS nanocrystals.[14,15] Increasing absorption at higher energies and strong photoluminescence peaking near 1100 nm suggests quantum confinement and band-edge luminescence consistent with 4 nm PbS nanocrystals.[16] Figure 3b shows additional photoluminescence spectra for four samples under excitation at 830 nm. When an extended (7 h) incubation was performed at room temperature, the photoluminescence spectrum in Figure 3b (red curve) was obtained, and a photoluminescence quantum efficiency of 1.5 ± 0.5 % was measured. This spectrum exhibits an additional spectral feature red-shifted relative to the principal photoluminescence peak; we associate it with trap-state emission which accounts for the weakened, red-shifted luminescence. When the standard (20 min) incubation protocol was followed at room temperature, no measurable luminescence was observed. The black curves in Figure 3b are photoluminescence spectra for samples synthesized at temperatures ranging from 70 to 95 °C. At higher temperatures, the increasing incidence of denaturation bubbles makes potential binding sites available; this facilitates better surface passivation and increases band-edge photoluminescence, and, thus, photoluminescence quantum efficiency. Across a set of twenty samples synthesized over this temperature range, an average absolute quantum efficiency of 9 ± 1 % was measured. The highest quantum efficiency measured was 11.5 ± 1 %. Spectra were identical across all of these synthetic trials.

Stored in aqueous solution, samples synthesized using the optimized protocol retained over 80 % of their initial quantum efficiency for over one month following synthesis. Across a wide range of synthetic conditions little variation in photoluminescence spectra was observed, as illustrated by the histogram in the inset of Figure 3b. Photoluminescence spectra are characteristically centered at 1085 nm and are 135 meV wide at half-maximum. Occasional batches were produced that exhibited the red spectral feature previously ascribed to trap-state emission in Figure 3a; these spectra were consistently accompanied by poor quantum efficiencies.

Samples were diluted in standard blood plasma (1:1 by volume) and held at 37 °C to study the effect of standard plasma on sample ageing; in the best samples, a luminescence quantum efficiency half-life of one week was observed. In samples that exhibited the additional spectral feature red-shifted relative to the main photoluminescence peak, corresponding to low initial quantum efficiency, combining with blood plasma increased their quantum efficiency and resulted in a growth in intensity at the main peak emission wavelength.

We prepared thin solid films from DNA-grown nanoparticles and measured the photoluminescence quantum efficiency of these to be 8 ± 1 %. This is in striking contrast to organometallic-route PbS nanoparticles, which exhibit 10–20 % quantum efficiencies in solution, but which, when subsequently formed into pure or nanocomposite quantum-dot–polymer films, degrade to 0.5–1.5 % photoluminescence quantum efficiency.[17–19] This has been variously attributed to the loss of surface passivation during film formation and to interdot interactions when closely packed in the solid state. From the interdot spacing seen in the EFTEM of Figure 2a and from the preservation of luminescence quantum efficiency observed in films, DNA appears to keep the nanocrystals separated and passivated in the solid state.

In conclusion, we have reported the first synthesis of efficient photoluminescent quantum dots via growth on a DNA template. The nanoparticles produce light in the infrared wavelength range in which deep penetration into living tissue and low autofluorescence have been demonstrated. The materials have high photoluminescence quantum efficiencies in aqueous solution and are stable in plasma at body temperature for over one week. When formed into extremely smooth (< 4 nm surface roughness) thin solid films, the materials retain their photoluminescence quantum efficiency, in stark contrast to infrared-emitting nanoparticles formed using the organometallic route.

Experimental

Synthesis: All solutions were prepared by using deionized water (18.2 MΩ cm). Type I fibrous highly polymerized (20 kb) DNA sodium salt (35 mg) from calf thymus (42 % cytosine-guanine base pairs) was dissolved in water (5 mL) and incubated under nitrogen at temperatures ranging from 20–100 °C. Syntheses were performed under vigorous stirring (1250 rpm) in a three-neck flask equipped with a condenser and thermocouple. With the solution held at the incubation temperature, a lead nitrate solution ($Pb(NO_3)_2$, 3.0 mL, 1.0×10^{-2} M) was added dropwise over 20 min using a syringe pump. A stoichiometric amount of sodium sulfide was added through a single injection, resulting in a dark red solution. The heating mantle was removed and the reaction flask allowed to cool to room temperature.

Syntheses carried out in the absence of DNA resulted in the rapid formation of aggregated bulk particles, which precipitated from the solution. These materials provided no measurable luminescence.

Obtaining DNA-supported PbS quantum dots depended on lead and sulfur precursor concentrations. We investigated the effects of varying i) the concentration of DNA salt, ii) the concentrations of lead and sulfur precursors, and iii) the Pb/S molar ratio at temperatures over the range from 20 to 100 °C. The DNA concentration was varied from 1.0 to 7.0 mg mL^{-1}. The highest photoluminescence efficiency and reproducibility were observed for the DNA concentration range of 5.0–7.0 mg mL^{-1}. The Pb/S molar ratio, when varied from 1:0.7 to 1:8, did not affect the photoluminescence quantum efficiency. However, when the Pb/S molar ratio was held constant at 1:1, increasing the precursor concentrations led to increased photoluminescence intensity up to a concentration of 5×10^{-5} moles in our 5 mL reaction volume, beyond which precipitation occurred.

Determination of Absolute Photoluminescence Quantum Efficiency: The experimental procedure and method of analysis that allow the absolute determination of photoluminescence quantum efficiency was described in [20]. The method begins with calibration of the spectral response of the entire system with the aid of an emission monochromator equipped with a tungsten-halogen lamp and calibrated photodetector. We acquired calibrated power spectra in three configurations of the integrating sphere: empty sphere, sample in sphere and indirect illumination, sample in sphere and direct illumination. We used this set of measurements to determine the absolute photoluminescence quantum efficiency, as they account for such effects as scattering from the sphere walls, absorption of the scattered light, and reabsorption of light emitted from the sample and subsequently scattered from the sphere walls.

Film Formation: Uniform films occupying ~5 cm× 5 cm were prepared by depositing 1000 μL of solution on a glass substrate. The solution was confined by inert sidewalls and allowed to dry. Films with thicknesses ranging from 1–3 μm were fabricated. Atomic force microscopy revealed a surface roughness of 4 nm over a 1 μm × 1 μm region. The films exhibited interference fringes apparent in the absorption spectrum. Fabry–Perot fringe spacing indicated a phase index of 1.69 ± 0.03 between 1200 and 1500 nm. The films formed the core of planar waveguides on silica (refractive index ~1.5), in which light is well-confined to the DNA–PbS material.

TEM and EFTEM: TEM images were acquired using the transmitted- and scattered-electron detectors of a HD-2000 scanning transmission electron microscope operating at 200 kV (Hitachi). EFTEM imaging was performed with a Tecnai 20 (FEI, Eindhoven) transmission electron microscope equipped with an electron imaging spectrometer (Gatan, Pleasanton, CA) operated at 200 kV. Phosphorus-enhanced images were collected at 155 eV energy loss, just beyond the $L_{II,III}$ phosphorus ionization edge. A 20 eV energy window was used. Bright-field images were collected at zero loss. For EFTEM sample preparation, carbon films 3–5 nm in thickness were floated onto 1000-mesh grids. The DNA–PbS solution was diluted in a mixture of Hepes (10 mM, pH 8) and $MgCl_2$ (1 mM). A small drop was placed onto the grid and allowed to adsorb to the film for 5 min. The grid was then rinsed three times with filtered distilled water and allowed to dry in air.

Received: July 27, 2004
Final version: May 4, 2005

[1] A. P. Alivisatos, *Nat. Biotechnol.* **2004**, *22*, 47.
[2] S. Kim, Y. T. Lim, E. G. Soltesz, A. M. De Grand, J. Lee, A. Nakayama, J. A. Parker, T. Mihaljevic, R. G. Laurence, D. M. Dor, L. H. Cohn, M. G. Bawendi, J. V. Frangioni, *Nat. Biotechnol.* **2004**, *22*, 93.
[3] M. A. Hines, P. Guyot-Sionnest, *J. Phys. Chem.* **1996**, *100*, 468.
[4] D. Gerion, F. Pinaud, S. C. Williams, Q. J. Parak, D. Zanchet, S. Weiss, A. P. Alivisatos, *J. Phys. Chem. B* **2001**, *105*, 8861.
[5] S. Kim, M. G. Bawendi, *J. Am. Chem. Soc.* **2003**, *125*, 14 652.
[6] C. A. Mirkin, R. L. Letsinger, R. C. Mucic, J. J. Storhoff, *Nature* **1996**, *382*, 607.
[7] J. L. Coffer, S. R. Bigham, R. F. Pinizzotto, H. Yang, *Nanotechnology* **1992**, *3*, 69.
[8] J. L. Coffer, S. R. Bigham, X. Li, R. F. Pinizzotto, Y. G. Rho, R. M. Pirtle, I. L. Pirtle, *Appl. Phys. Lett.* **1996**, *69*, 3851.
[9] T. Torimoto, M. Yamashita, S. Kuwabata, T. Sakata, H. Mori, H. Yoneyama, *J. Phys. Chem. B* **1999**, *103*, 8799.
[10] S. R. Bigham, J. L. Coffer, *Colloids Surf. A* **1995**, *95*, 211.
[11] S. R. Bigham, J. L. Coffer, *J. Cluster Sci.* **2000**, *11*, 359.
[12] A. A. Patel, F. X. Wu, J. Z. Zhang, C. L. Torres-Martinez, R. K. Mehra, Y. Yang, S. H. Risbud, *J. Phys. Chem. B* **2000**, *104*, 11 598.
[13] M. J. Hendzel, D. P. Bazett-Jones, *J. Microsc. (Oxford)* **1996**, *182*, 1.
[14] L. Bakueva, I. Gorelikov, S. Musikhin, X. S. Zhao, E. H. Sargent, E. Kumacheva, *Adv. Mater.* **2004**, *16*, 926.
[15] X. Zhao, I. Gorelikov, S. Musikhin, S. Cauchi, V. Sukhovatkin, E. H. Sargent, E. Kumacheva, *Langmuir* **2005**, *21*, 1086.
[16] F. W. Wise, *Acc. Chem. Res.* **2000**, *33*, 773.
[17] L. Bakueva, S. Musikhin, M. A. Hines, T. W. F. Chang, M. Tzolov, G. D. Scholes, E. H. Sargent, *Appl. Phys. Lett.* **2003**, *82*, 2895.
[18] J. S. Steckel, S. Coe-Sullivan, V. Bulovic, M. G. Bawendi, *Adv. Mater.* **2003**, *15*, 1862.
[19] E. H. Sargent, *Adv. Mater.* **2005**, *17*, 515.
[20] T.-W. F. Chang, A. Maria, P. W. Cyr, V. Sukhovatkin, L. Levina, E. H. Sargent, *Synth. Met.* **2005**, *148*, 257.

Fabrication of Three-Dimensional Nanostructures Using Reactive Polymer Nanosheets**

By *Yuko Kado*, *Masaya Mitsuishi*, and *Tokuji Miyashita**

The colors of nature surround us. Different aspects of the interaction between light and matter produce them. The most common is light interacting with colored pigments. However, some living things, such as butterflies, beetles, birds, and tropical fish, exhibit color and have unique display systems that use different interactions. Structural color is responsible for their brilliant colors. Structural color originates from the interference, diffraction, scattering, etc. of light reflected from surface structures. Surprisingly, instead of pigments, they have periodically ordered and highly organized microscale or nanoscale structures on their body surfaces—typically scales or wings.[1–4] Several factors determine structural color and its intensity: the thickness and spacing of the layers of scales or epicuticles, the number of these layers, and the angle of incoming light. For example, color resulting from light interference (interference color) is determined by the thickness meeting the Bragg condition. Interference color is shown when a layer, whose thickness is of the order of 100 nm, is on a flat and lustrous (highly reflective) surface. Therefore, nanoscale control is required for surface structures to artificially create such structural color and to apply similar structures to various advanced devices.[5–8]

For this structural color and for miniaturization of various devices, a great deal of money, time, and effort have been devoted to developing techniques to fabricate two-dimensional (2D) and three-dimensional (3D) nanostructures.[9–11] In particular, nanostructures comprised of organic materials have been in demand for the last few decades because of their processability, ease of functionalization, light weight, flexibility, and so on. For this purpose, various organic thin films and organic thin layers are widely used for producing microdevices and nanodevices under severe space constraints.[12] For the deposition of organic thin layers onto solid substrates, representative organic ultrathin films are self-assembled monolayers (SAMs);[13–15] polymer brushes made by free-radical polymerization and living radical polymerization, such as atom trans-

[*] Prof. T. Miyashita, Dr. Y Kado, Dr. M. Mitsuishi
Institute of Multidisciplinary Research for Advanced Materials (IMRAM)
Tohoku University
Katahira 2-1-1, Aoba-ku, Sendai 980-8577 (Japan)
E-mail: miya@tagen.tohoku.ac.jp

[**] The authors thank the Nanotechnical Lab. IMRAM, Tohoku University for the use of AFM. This work was supported by a Grant-in-Aid for Scientific Research (No. 14205130) from the Japanese Ministry of Education, Culture, Sports, Science and Technology. Supporting Information is available online from Wiley InterScience or from the author.

 DOI: 10.1002/adma.200500884